The Cerebellum (2021) 20:41–53
https://doi.org/10.1007/s12311-020-01179-7

ORIGINAL ARTICLE

Antisense Oligonucleotide Therapy Targeted Against *ATXN3* Improves Potassium Channel–Mediated Purkinje Neuron Dysfunction in Spinocerebellar Ataxia Type 3

David D. Bushart[1] · Annie J. Zalon[1] · Hongjiu Zhang[2,3] · Logan M. Morrison[1,4] · Yuanfang Guan[2] · Henry L. Paulson[1] · Vikram G. Shakkottai[1,5] · Hayley S. McLoughlin[1]

Published online: 13 August 2020

Abstract

Spinocerebellar ataxia type 3 (SCA3) is the second-most common CAG repeat disease, caused by a glutamine-encoding expansion in the ATXN3 protein. SCA3 is characterized by spinocerebellar degeneration leading to progressive motor incoordination and early death. Previous studies suggest that potassium channel dysfunction underlies early abnormalities in cerebellar cortical Purkinje neuron firing in SCA3. However, cerebellar cortical degeneration is often modest both in the human disease and mouse models of SCA3, raising uncertainty about the role of cerebellar dysfunction in SCA3. Here, we address this question by investigating Purkinje neuron excitability in SCA3. In early-stage SCA3 mice, we confirm a previously identified increase in excitability of cerebellar Purkinje neurons and associate this excitability with reduced transcripts of two voltage-gated potassium (K_V) channels, *Kcna6* and *Kcnc3*, as well as motor impairment. Intracerebroventricular delivery of antisense oligonucleotides (ASO) to reduce mutant ATXN3 restores normal excitability to SCA3 Purkinje neurons and rescues transcript levels of *Kcna6* and *Kcnc3*. Interestingly, while an even broader range of K_V channel transcripts shows reduced levels in late-stage SCA3 mice, cerebellar Purkinje neuron physiology was not further altered despite continued worsening of motor impairment. These results suggest the progressive motor phenotype observed in SCA3 may not reflect ongoing changes in the cerebellar cortex but instead dysfunction of other neuronal structures within and beyond the cerebellum. Nevertheless, the early rescue of both K_V channel expression and neuronal excitability by ASO treatment suggests that cerebellar cortical dysfunction contributes meaningfully to motor dysfunction in SCA3.

Keywords Ataxia · Antisense oligonucleotide · Potassium channel · Purkinje neuron · Cerebellum

Introduction

Spinocerebellar ataxia type 3 (SCA3), also known as Machado-Joseph disease, is the most common dominantly inherited ataxia [1–3]. Pathologically, the disease is characterized by progressive neurodegeneration and neuronal loss in specific brain regions including the deep cerebellar nuclei (DCN), brainstem nuclei, and vestibular nuclei [4, 5]. In contrast to many other SCAs, in SCA3, the degree of cerebellar cortical degeneration tends to be modest, with more than 75% of Purkinje neurons often preserved [1]. Nevertheless, clinical features of SCA3 include prominent, progressive ataxia characterized by difficulties in gait, balance, and coordination, ultimately resulting in death [6]. Although cerebellar Purkinje neuron degeneration is not a major feature of SCA3

David D. Bushart and Annie J. Zalon contributed equally to this work.

✉ Vikram G. Shakkottai
vikramsh@med.umich.edu

✉ Hayley S. McLoughlin
hayleymc@med.umich.edu

[1] Department of Neurology, University of Michigan, 109 Zina Pitcher Pl., Ann Arbor, MI 48109, USA

[2] Department of Computational Medicine & Bioinformatics, University of Michigan, Ann Arbor, MI 48109, USA

[3] Microsoft, Inc., Bellevue, WA 98004, USA

[4] Neuroscience Graduate Program, University of Michigan, Ann Arbor, MI 48109, USA

[5] Department of Molecular & Integrative Physiology, University of Michigan, 109 Zina Pitcher Pl., Ann Arbor, MI 48109, USA

despite this prominent ataxia, it remains unclear whether dysfunction of the cerebellar cortex contributes to disease.

SCA3 is caused by pathologic expansion of a CAG repeat in the *ATXN3* gene that encodes an expanded polyglutamine sequence in the ATXN3 protein. No disease-modifying therapies yet exist for SCA3. In knockout mice, no deleterious consequences of ATXN3 loss are observed [7]; thus, gene suppression strategies targeting *ATXN3* represent an attractive therapeutic option for SCA3. CNS-delivered antisense oligonucleotides (ASOs) can successfully reduce the level of *ATXN3* transcripts in SCA3 mice, resulting in marked reduction of ATXN3 protein expression throughout disease-relevant brain regions, including the brainstem and cerebellum [8–10]. In this study, we use ASOs to address the role of cerebellar cortical dysfunction in SCA3 to determine its relevance as a target of ASO therapy.

In mouse models of several polyglutamine SCAs, cerebellar Purkinje neuron dysfunction is associated with early deficits in motor function. Alterations in Purkinje neuron spike frequency or regularity appear at the onset of motor impairment in mouse models of SCA1 [11], SCA2 [12, 13], SCA3 [14], SCA6 [15], and SCA7 [16]. Ion channel dysregulation contributes to altered Purkinje neuron spiking in these models [17]. In light of the prominent degeneration of cerebellar Purkinje neurons in human SCA1, SCA2, SCA6, and SCA7, these early Purkinje neuron abnormalities in mouse models support the view that neuronal dysfunction contributes to the degenerative process [1, 5]. In contrast, the relative preservation of Purkinje neurons in human SCA3 suggests a less important role for cerebellar cortical dysfunction in motor impairment. Instead, prominent degeneration of cerebellar nuclei suggests that a loss of cerebellar output is principally responsible for cerebellar signs in SCA3 [4, 5]. Despite this neuropathological evidence, voltage-gated potassium (K_V) channel dysfunction has been proposed to underlie Purkinje neuron hyperexcitability in a mouse model of SCA3 [14]. These observations suggest that cerebellar Purkinje neurons, despite their relatively minor degeneration in SCA3 compared with other SCAs, may experience a period of neuronal dysfunction that plays an important functional role in motor impairment.

In the present study, we investigate changes in cerebellar Purkinje neuron physiology that occur in a mouse model of SCA3 and examine whether ASO treatment to rescue changes in cerebellar cortical dysfunction is associated with improvement in motor dysfunction. We confirm a previously observed increase in cerebellar Purkinje neuron excitability and identify several K_V channel transcripts that are reduced in association with these changes in physiology. ASO-mediated gene suppression of ATXN3 rescued both the hyperexcitability phenotype in SCA3 mice and the change in transcript levels of the underlying K_V channels, providing insight into the basis of aberrant spiking. Our results suggest that cerebellar cortical dysfunction contributes to early motor dysfunction in SCA3, but the absence of further changes in Purkinje neuron physiology as motor dysfunction worsens in later-stage disease implies that this later motor impairment is mostly driven by regions beyond the cerebellar cortex.

Materials and Methods

Animals

All animal procedures were approved by the University of Michigan Institutional Animal Care and Use Committee (IACUC). Procedures were conducted in accordance with the U.S. Public Health Service's Policy on Humane Care and Use of Laboratory Animals.

Homozygous YACMJD84.2Q-C57BL/6 transgenic mice (referred to simply as "SCA3 mice" in this manuscript) [18] and wild-type littermate controls were housed together with a maximum of five animals per cage and exposed to a standard 12-h light/dark cycle with food and water ad libitum. Prior to weaning, DNA was isolated from mouse tail biopsies to determine genotype using quantitative real-time qPCR as previously described [9]. Fragment analysis was used to assess human ATXN3 repeat length (Laragen, San Diego, CA), with a threshold of 75Q or greater included in studies. Genotypes were confirmed postmortem. For this study, animals were age- and sex-matched, and euthanized at either 8, 16, or 65 weeks of age for biochemical analysis following an ASO or vehicle treatment at 8 weeks of age. At the time of harvesting, tissue was macrodissected to isolate the cerebellum for biochemical assessment as previously described [9]. Mice designated for electrophysiological recordings were harvested at 16 and 65 weeks of age. An experimenter was blinded to the genotype and treatment condition of all mice for all electrophysiology and behavioral assessments.

Antisense Oligonucleotides

The antisense oligonucleotide (ASO) targeting *ATXN3* (ASO-5; GCATCTTTTCATTACTGGC) used in this study was previously described [8], with a gapmer design that targets the 3′ untranslated region of both human and mouse *ATXN3*. ASOs were synthesized as previously described [9] and solubilized in filtered PBS.

Surgical Delivery of Antisense Oligonucleotides

Mice were stereotaxically injected at 8 weeks of age with either 10 μL of ASO-5 (700 μg) or PBS vehicle treatments into the right lateral ventricle as previously described [9]. In the 65-week-old mice, vehicle injections were performed at 8 and 22 weeks of age after which point treatment was

discontinued. Mice were monitored postoperatively for grooming activity, weight, and home cage activity for up to 10 days.

RNA Isolation and Quantitative Real-time PCR

Dissected whole cerebellar tissue was homogenized and total RNA was isolated using TRizol reagent according to the manufacturer's instructions (Invitrogen, Carlsbad, CA). Reverse transcription on 0.5 to 1 μg of total RNA was performed using the iScript cDNA synthesis kit (Bio-Rad, Hercules, CA) according to the manufacturer's instructions. The resulting cDNA was diluted 1:20 in nuclease-free water. iQ SYBR green (Bio-Rad) or Taqman (Thermo Fisher) quantitative polymerase chain reaction (qPCR) was conducted per the manufacturer's instructions and analyzed to determine the average-adjusted relative quantification using the following primer sets/probes:

1. Human *ATXN3* (5′-GAAGCTGACCAACTCCTGC-3′; 5′-CTTCTAACACTCGTTCCAGG-3′).
2. *Beta Actin* (5′-GAACGGACAGCCATGGGCGGG-3′; 5′-GTGTGTCCCCAAGCCCCACG-3′).
3. *Kcnc3* (5′-TTTTTGAGGACCCCTACTCG-3′; 5′-ATGAAGCCCTCGTGTGTCTC-3′).
4. *Kcna6* (Thermo Fisher; Cat # Mm00496625).

RNA Sequencing and Gene Expression Analysis

Mice with average CAG repeat lengths of ≥ 75 were used for this study. High-quality extracted wild-type and SCA3 cerebellar RNA was verified prior to sequencing, with all samples in study exhibiting a RIN greater than 7. RNA samples were submitted to the University of Michigan Bioinformatics Core for library generation (Illumina TruSeq) and sequenced on Illumina HiSeq 4000 (75 × 75 pair-end, 4 lanes). Merging ENSEMBL 94 human ATXN3 reference cDNA sequences (Oct 2018, GRCh38p12) and ENSEMBL 94 mouse reference cDNA sequences (Oct 2018, GRCm38p6) were used to create a synthetic reference transcriptome.

RNA-seq data were mapped to the synthetic reference sequences using Kallisto 0.45 and the resulting transcript quantification was then fed to Sleuth 0.30 for differential expression analysis, aggregated by the corresponding genes of the transcripts. Genes with expression levels less than 5 transcripts per million (TPM) in more than 25% of the analyzed cerebellar samples at each time point (8, 16, or 65 weeks) were discarded from further analysis. Sleuth assessed the gene-wise statistical significance of the hypotheses that a gene is differentially expressed in wild-type samples compared with transgenic samples at each time point. Genes with q values less than 0.05 were considered differentially expressed genes using the Benjamini-Hochberg corrections test.

Analysis of In Situ Hybridization Data

Images used for the analysis of in situ hybridization data were obtained from the Allen Expression Atlas [19]. Three consecutive images in the sagittal orientation were downloaded from the Allen Expression Atlas for each analyzed gene. The beginning of the series was defined as the most medial section that contained the fastigial nucleus, and the two images directly lateral to the first section were also chosen. The probe IDs for analyzed genes were as follows: *Kcna1* (69735688), *Kcna2* (69257999), *Kcna6* (70523814), *Kcnc1* (70724858), *Kcnc3* (69735694), *Kcnd3* (74431640), *Calb1* (70919860), *Gapdh* (70276861). Images were transformed to 16-bit grayscale using ImageJ (National Institutes of Health) then the background was subtracted uniformly for all images within a series. A freeform box was drawn around the Purkinje neuron somatic layer for the entire length of lobule 5 or lobule 10, and a corresponding section of the molecular layer directly next to these cerebellar regions was also selected. Freeform boxes were also drawn around the medial cerebellar nuclei and the pontine gray matter. Reported values are for average pixel intensity within these analyzed regions.

Open-Field Motor Evaluation

Motor and exploratory behaviors were measured at 16 weeks old using a photobeam activity system open-field apparatus (San Diego Instruments, San Diego, CA). Mice were placed in this apparatus for a 30-min trial. Total activity was calculated by measuring the total number of x-/y-axis beam breaks while exploratory/rearing activity was calculated by measuring total z-axis beam breaks.

Patch-Clamp Electrophysiology

Patch-clamp recordings were performed as previously described [20]. Briefly, mice were euthanized under deep isoflurane anesthesia and brains were placed in pre-warmed (33 °C) artificial cerebrospinal fluid (aCSF) bubbled with carbogen (95% O_2, 5% CO_2). aCSF contained (in mmol/L): 125 NaCl, 3.8 KCl, 26 $NaHCO_3$, 1.25 NaH_2PO_4, 2 $CaCl_2$, 1 $MgCl_2$, 10 glucose. Parasagittal cerebellar sections were prepared in carbogen-bubbled aCSF at 33–35 °C to 300-μM thickness using a vibratome (Leica Biosystems, Buffalo Grove, IL). Slices rested for 45 min before recording.

For all patch-clamp recordings, borosilicate glass pipets were pulled to 3–4 MΩ resistance and filled with an

internal solution containing (in mmol/L): 119 K-gluconate, 2 Na-gluconate, 6 NaCl, 2 $MgCl_2$, 0.9 EGTA, 10 HEPES, 14 Tris-phosphocreatine, 4 Mg-ATP, 0.3 Tris-GTP, at pH 7.3 and osmolarity 290 mOsm. Recordings were performed at 33 °C in carbogen-bubbled aCSF at a flow rate of 2–3 mL/min 1–5 h after slice preparation. Recordings were performed with an Axopatch 200B amplifier, Digidata 1440A interface, and pClamp-10 software (Molecular Devices, San Jose, CA). Data were acquired at 100 kHz in fast current-clamp mode and filtered at 2 kHz. A 10-mV liquid junction potential correction was applied to voltage traces.

Strict inclusion criteria were used for electrophysiological recordings. Purkinje neurons chosen for recording were morphologically identified as intact, teardrop shaped, and had no visible nucleolus or membrane blebbing. All neurons chosen for recording were noted to be spontaneously firing. Recordings were performed with the experimenter blind to genotype. For whole-cell recordings, cells were rejected if the series resistance exceeded 15 MΩ or changed by more than 20% during the recording.

Electrophysiology data was processed and analyzed in ClampFit software (Molecular Devices, San Jose, CA). For AHP analysis, cells were held at − 80 mV and injected with increasing steps of depolarizing current until a full 1-s spike train was evoked. AHP analysis was performed on the first spike of the full train. Maximum depolarization d*V*/d*t* and repolarization d*V*/d*t* were derived from the same spike used for AHP analysis. Spike regularity was measured as the coefficient of variation (CV) of the interspike interval (ISI), defined as (ISI standard deviation)/(ISI mean). Spike half-width is a measure of spike width at 50% of peak amplitude from threshold, as defined by ClampFit. The steady-state membrane potential was measured at the 50% point between all spikes over a 30-s period and is presented as a mean value. All other parameters are generated by ClampFit or derived from data extracted from ClampFit analysis.

Data Analysis and Statistics

All data were subjected to an outlier test, and the final data presented in the figures and statistical analyses have had statistical outliers removed. Statistical analyses were performed using Prism 8.0 (GraphPad Software, La Jolla, CA). Statistical significance was tested using analysis of variance (ANOVA) with a Holm-Sidak or Tukey correction for multiple comparisons, or by two-tailed Student's *t* test. Variability about the mean is expressed as mean ± standard error of the mean. An alpha level of 0.05 was used to denote statistical significance for each test.

Results

Longitudinal Changes in Expression of Voltage-Gated Potassium Channel Genes Enriched in Cerebellar Purkinje Neurons

Although degeneration of the cerebellar cortex is prominent in most of the CAG repeat SCAs (including SCAs 1, 2, 6, and 7), SCA3 differs in that cerebellar Purkinje neurons are relatively preserved, as assessed by volumetric MRI and postmortem tissue analysis [4, 5]. In mouse models of SCA3, however, studies show that Purkinje neuron dysfunction may contribute to motor impairment [8, 14]. In these studies, K_V channel dysfunction was proposed to underlie abnormal Purkinje neuron firing. However, changes in Purkinje neuron physiology were not uniform across these studies, and the specific K_V targets contributing to altered firing were not fully determined.

We sought to define the specific K_V channel contribution to Purkinje neuron firing abnormalities in SCA3. We analyzed whole cerebellar RNA sequencing data from homozygous mice of the YACMJD84.2Q-C57BL/6 model of SCA3 [18] (referred to here as "SCA3" mice) at three time points: 8 weeks (early-stage symptomatic), 16 weeks (mid-stage symptomatic), and 65 weeks (late-stage symptomatic) of age. We focused our analysis on transcript reads for K_V channels either with known enrichment in cerebellar Purkinje neurons [21–24] or associated with human mutations causing cerebellar ataxia [25–28]. These channels include *Kcna1* (encoding K_V1.1), *Kcna2* (K_V1.2), *Kcna6* (K_V1.6), *Kcnc1* (K_V3.1), *Kcnc3* (K_V3.3), and *Kcnd3* (K_V4.3) (Fig. 1a–f). The only gene that showed reduced expression at 8 weeks of age was *Kcna6* (Fig. 1c), and only *Kcna6* and *Kcnc3* (Fig. 1e) showed reduced expression at 16 weeks of age, a mid-stage symptomatic time point in SCA3 mice. All transcripts except *Kcnd3* (Fig. 1f) showed reduced expression at 65 weeks of age, an advanced stage of disease in SCA3 mice [29].

Motor symptoms appear in SCA3 mice by 6 weeks of age and become more prominent by 12 weeks [29]. Based on work in other models of SCA, ion channels that show reduced expression early in the disease are more likely to contribute to motor impairment [17]. Early changes in physiology are tractable therapeutic targets in SCA3 and other ataxias, which could be accomplished by directly modulating the implicated ion channels [17, 30] or potentially by knocking down *ATXN3* expression [3]. A compelling strategy to reduce polyglutamine-expanded ATXN3 involves the use of non-allele specific ASOs targeting *ATXN3* [8, 9]. Therefore, we sought to explore the contribution of K_V channel dysfunction to motor impairment at 16 weeks of age, a time at which changes in Purkinje neuron spiking have been identified in heterozygous SCA3 mice and when anti-*ATXN3* ASO treatment led to motor rescue

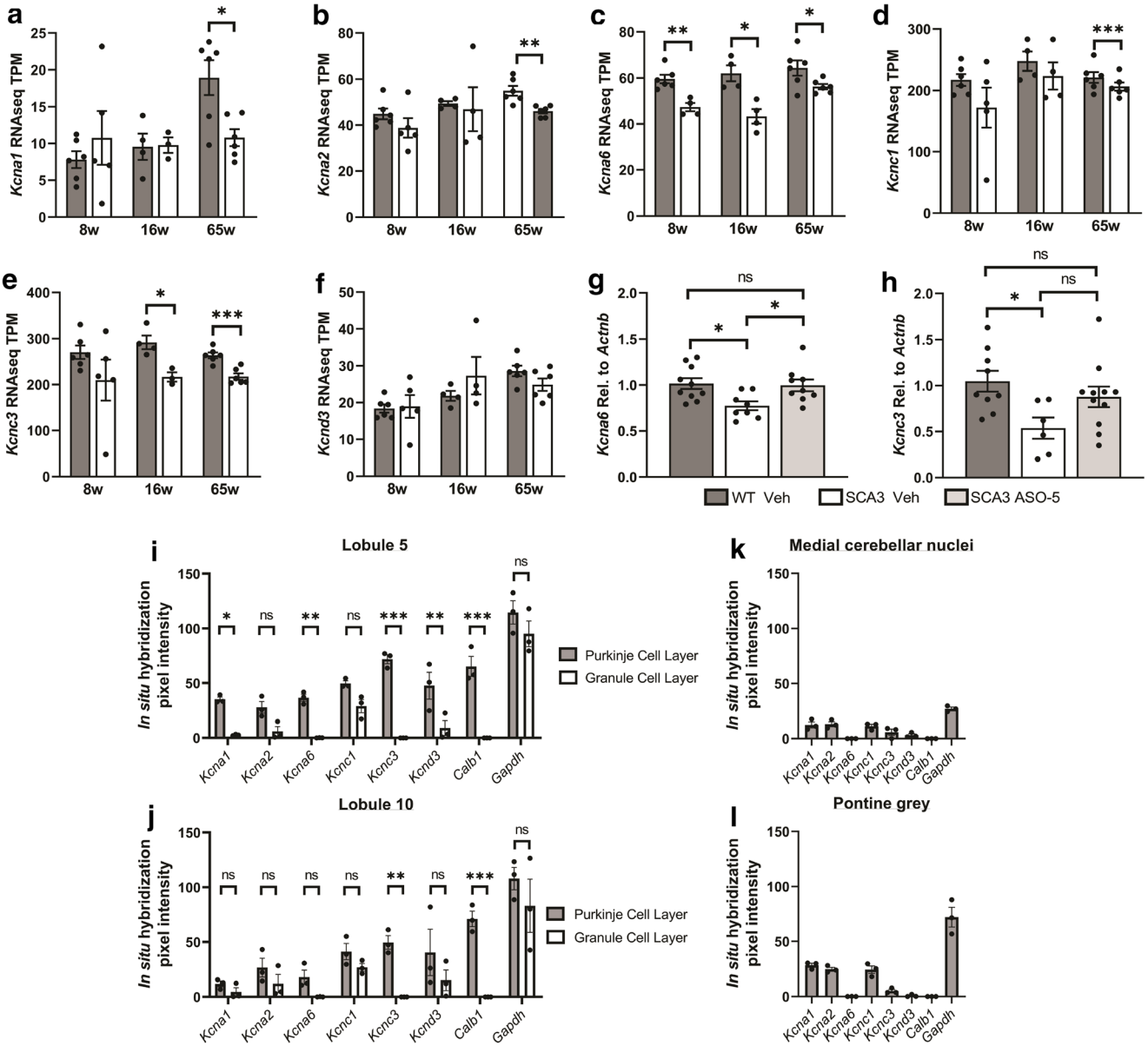

Fig. 1 Longitudinal changes in expression of potassium channel genes highly enriched in cerebellar Purkinje neurons. Average RNA-Seq transcript per million (TPM) of **a** *Kcna1*, **b** *Kcna2*, **c** *Kcna6*, **d** *Kcnc1*, **e** *Kcnc3*, and **f** *Kcnd3* in 8-, 16-, and 65-week-old WT and SCA3 cerebella. Quantitative real-time PCR validation in 16-week-old vehicle- and ASO-5-treated mice of differentially regulated genes, **g** *Kcna6* and **h** *Kcnc3*. **i** Analysis of in situ hybridization data in the anterior cerebellum, obtained from the Allen Brain Atlas [19]. Similar to (**i**), in situ hybridization data was analyzed from the Allen Brain Atlas in the nodular zone of the cerebellum (**j**), the medial cerebellar nuclei (**k**), and the pontine gray matter (**l**). * = $p < 0.05$, ** = $p < 0.01$, *** = $p < 0.001$. Two-tailed Student's *t* test (**a**–**f**), two-tailed Student's *t* test with Bonferroni correction for multiple comparisons (**i**, **j**), one-way ANOVA (**g**, **h**)

[8]. Leveraging our experience with ASO-mediated knockdown of ATXN3, we assessed whether ASO treatment has an impact on K_V channel expression.

At 16 weeks of age, reduction in *Kcna6* and *Kcnc3* gene expression was confirmed in SCA3 mice by quantitative PCR (Fig. 1g, h). In vehicle-treated SCA3 (SCA3 Veh) mice, both *Kcna6* and *Kcnc3* were significantly reduced when compared with that in vehicle-treated wild-type (WT Veh) mice. *Kcna6* expression was restored to WT levels in ASO-5-treated SCA3 (SCA3 ASO-5) mice (Fig. 1g), while *Kcnc3* expression was partially restored (Fig. 1h). ASO-5, a non-allele specific anti-*ATXN3* ASO, is well tolerated in mice, distributes widely throughout the CNS, and effectively reduces mutant and endogenous ATXN3 as well as high molecular weight aggregated species of ATXN3 [9]. Taken together, these data suggest that modest K_V channel dysregulation is present in SCA3 mice at 16 weeks of age and becomes more prominent by 65 weeks of age. In addition, ASO directed against *ATXN3* improves expression of the K_V channel genes affected early in disease.

RNA sequencing and qPCR studies in SCA3 mice were performed in whole cerebellar tissue. To determine which cerebellar regions are most likely to be impacted by reduced ion channel transcript expression, we performed an analysis of publicly available in situ hybridization data from wild-type C57BL/6 mice [19]. We analyzed relative expression of ion channel genes in the Purkinje neuron layer, granule cell layer, medial cerebellar nuclei (including fastigial nucleus), and pontine gray matter. In the anterior cerebellar lobules, we found a significantly enriched expression of *Kcna1*, *Kcna6*, *Kcnc3*, *Kcnd3*, and the Purkinje neuron marker *Calb1* (Fig. 1i). In the nodular zone, we found a significantly enriched expression of *Kcnc3* and *Calb1* (Fig. 1j). We also observed detectible levels of *Kcna1*, *Kcna2*, and *Kcnc3* in the medial cerebellar nuclei (Fig. 1k) and pontine gray matter (Fig. 1l), two structures outside of the cerebellar cortex that may influence cerebellar input and output [31] and are affected in human SCA3 [5]. Together, these data suggest that the ion channel transcripts affected in SCA3 cerebellum at 16 weeks of age are likely to impact Purkinje neuron function, particularly in the anterior cerebellum, and that a subset of these channels may be important for cerebellar network activity in structures beyond the cerebellar cortex.

Antisense Oligonucleotides Improve Purkinje Neuron Physiology in SCA3 Mice

In other rodent models of ataxia, changes in cerebellar ion channel expression or function are associated with altered Purkinje neuron firing. We therefore sought to determine whether reduced $K_V1.6$ and $K_V3.3$ channel expression results in differences in Purkinje neuron spiking in SCA3 mice. We also tested whether ASO administration improves changes in physiology that accompany K_V dysfunction in SCA3 mice.

We performed patch-clamp electrophysiology in acute cerebellar slices from SCA3 mice that had been injected with either ASO-5 or PBS vehicle control, comparing results with those in PBS vehicle-injected WT littermate controls at 8 weeks of age. Recordings were performed at 16 weeks of age, 8 weeks after ASO or vehicle injection. Because recent work indicates that Purkinje neuron physiology differs significantly in the anterior versus posterior cerebellar lobules [32], and these regions can be differentially affected in polyglutamine ataxia [16], we separately investigated the anterior and posterior cerebellar lobules (nodular zone).

In the anterior cerebellum, Purkinje neuron firing frequency (Fig. 2a) and regularity (Fig. 2b), as assessed by the coefficient of variation (CV) of the interspike interval (ISI), were not significantly changed among all groups. Previous studies have shown that $K_V3.3$ channel dysfunction can alter the action potential waveform [33, 34] or influence neuronal excitability [34, 35]. We therefore used whole-cell electrophysiological recordings to assess action potential characteristics. We observed no differences in action potential threshold across all groups (Fig. 2c), nor any gross changes in spike waveform (Fig. 2d). However, we detected an unexpected significant hyperpolarization of the afterhyperpolarization (AHP) and interspike interval (ISI) in SCA3 ASO-5 mice compared with both WT Veh and SCA3 Veh mice (Fig. 2e), although the absolute value of the change is relatively modest. There were no accompanying differences in spike half-width (Fig. 2f), maximum slope of depolarization (Fig. 2g), or maximum slope of repolarization (Fig. 2h). The spontaneous firing of Purkinje neurons makes it difficult to determine the resting membrane potential; however, the steady-state membrane potential, as represented as the halfway point between two subsequent spikes, was not significantly altered across all groups (Fig. 2i).

We similarly investigated Purkinje neuron firing in the nodular zone. Again, we detected no difference in firing frequency (Fig. 2j) or regularity (Fig. 2k) across all groups. Spike characteristics were also largely unchanged across all groups, including action potential threshold (Fig. 2l), action potential waveform (Fig. 2m), shape and decay of the AHP and ISI (Fig. 2n), maximum slope of depolarization (Fig. 2o), and maximum slope of repolarization (Fig. 2p). While spike half-width was slightly increased in SCA3 ASO-5–treated mice compared with SCA3 Veh–treated mice, it was not significantly different from WT Veh–treated mice (Fig. 2q). Additionally, the steady-state membrane potential was not altered among all groups (Fig. 2r). Taken together, these data indicate that action potential waveform is not significantly altered in SCA3 Purkinje neurons at 16 weeks of age in either the anterior cerebellum or the nodular zone.

Potassium channel dysfunction could influence neuronal excitability independently of gross changes in spike waveform. Therefore, we investigated the contribution of K_V channel dysfunction to neuronal excitability in SCA3 Purkinje neurons. In the anterior cerebellum, when Purkinje neurons were held at a hyperpolarized membrane potential of − 80 mV and injected with incrementally increasing steps of depolarizing current, SCA3 ASO-5 neurons required a lower amplitude of injected current to elicit depolarization block of repetitive spiking than WT Veh neurons (Fig. 3a). When we assessed the spike frequency in response to successive depolarizing current injection, SCA3 Veh neurons fired significantly more action potentials per sweep than WT Veh, while SCA3 ASO-5 neurons showed a decreased firing response to depolarizing current compared with both WT Veh and SCA3 Veh neurons (Fig. 3b). These alterations in spiking were not accompanied by changes in neuronal input resistance when measured between − 80 and − 75 mV (Fig. 3c).

In the nodular zone, the threshold of injected current to elicit depolarization block was significantly reduced in SCA3 Veh neurons compared with that in WT Veh neurons, while the reduction in required current to elicit depolarization

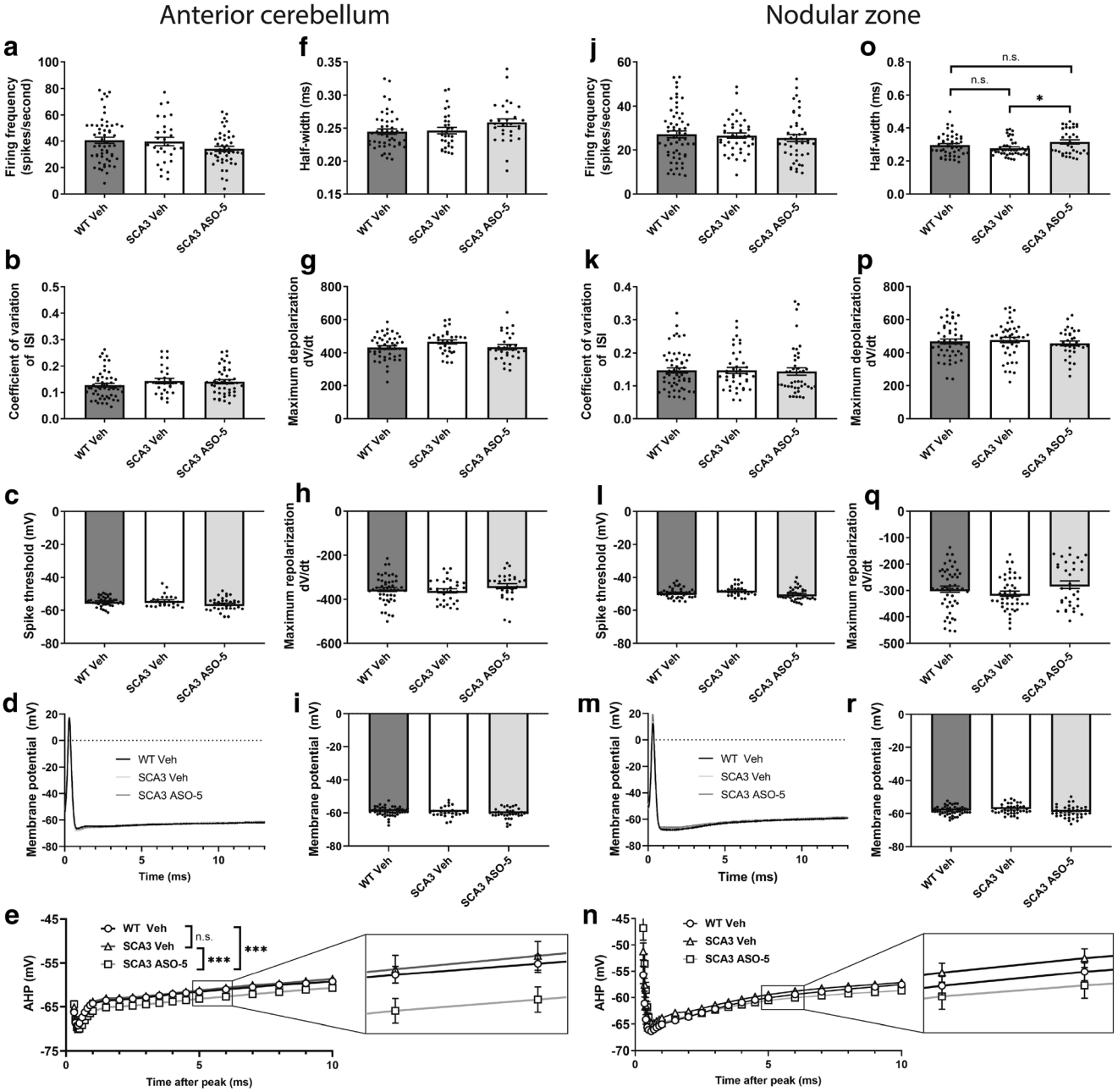

Fig. 2 Purkinje neuron spike waveform is not prominently affected in 16-week-old SCA3 mice. Patch-clamp recordings were performed in vehicle-treated WT, vehicle-treated SCA3, and ASO-5-treated SCA3 mice at 16 weeks of age. Panels **a**–**g** are from recordings in the anterior cerebellar lobules, while panels **h**–**n** are from recordings in the nodular zone. In the anterior cerebellum, **a** firing frequency is not altered among all groups, nor is **b** spike regularity, as denoted by coefficient of variation (CV) of the interspike interval (ISI). **c** Action potential threshold was not altered among all groups. **d** Representative overlays of individual spikes from WT Veh, SCA3 Veh, and SCA3 ASO-5 Purkinje neurons in the anterior cerebellum. **e** Shape and characteristics of the afterhyperpolarization (AHP) and ISI were not significantly altered between WT Veh and SCA3 Veh, while SCA3 ASO-5 resulted in hyperpolarization throughout the ISI. **f** Spike half-width, **g** maximum slope of depolarization, **h** maximum slope of repolarization, and **i** steady-state membrane potential were not altered among all groups. In the posterior cerebellum, **j** firing frequency is not altered among all groups, nor is **k** spike regularity as denoted by CV of the ISI. **l** Action potential threshold was not altered among all groups. **m** Representative overlays of individual spikes from WT Veh, SCA3 Veh, and SCA3 ASO-5 Purkinje neurons in the nodular zone. **n** Characteristics of the AHP and ISI were not altered among all groups. **o** Spike half-width was increased in SCA3 ASO-5 compared with SCA3 Veh, but this effect was modest and not significantly different from WT Veh. **P** Maximum slope of depolarization, **q** maximum slope of repolarization, and **r** steady-state membrane potential were not altered among all groups. * = $p < 0.05$, *** = $p < 0.001$, one-way ANOVA with Holm-Sidak correction for multiple comparisons, except in **e** and **n**, using two-way repeated measures ANOVA with Holm-Sidak correction for multiple comparisons

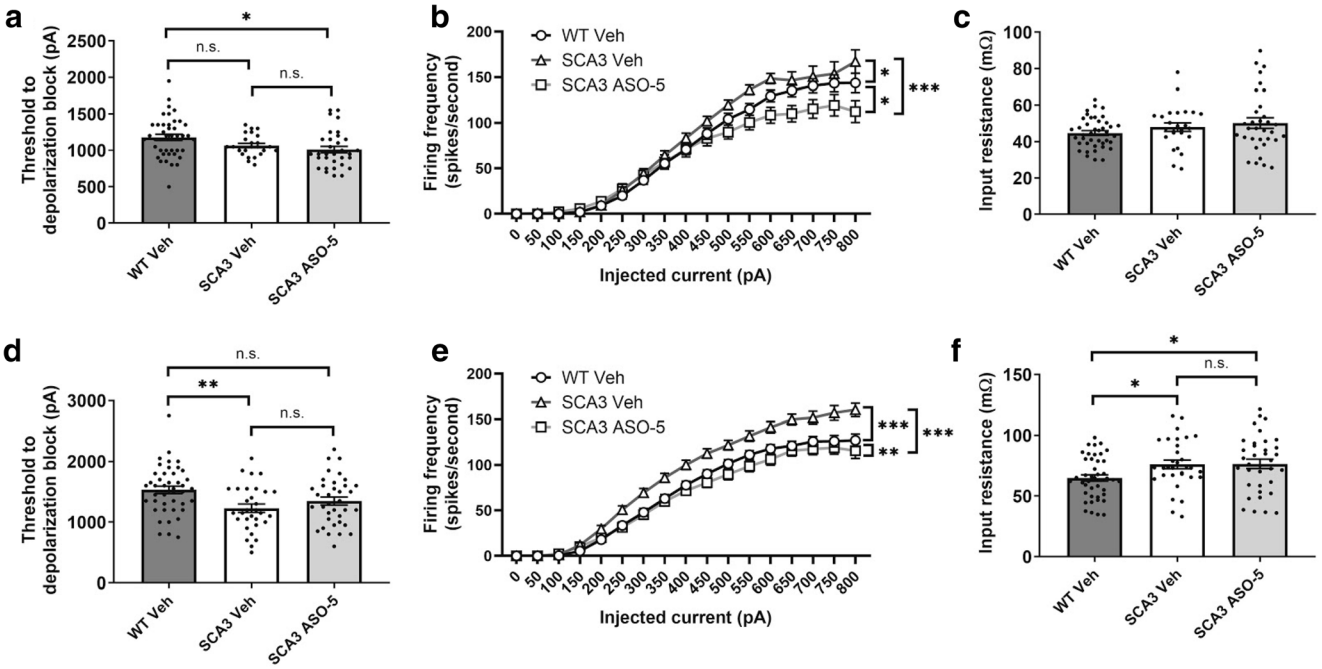

Fig. 3 Purkinje neuron hyperexcitability in 16-week-old SCA3 mice is rescued by ASO-5 treatment. Patch-clamp recordings were performed in vehicle-treated WT, vehicle-treated SCA3, and ASO-5-treated SCA3 mice at 16 weeks of age. Panels **a**–**c** are from recordings in the anterior cerebellar lobules, while panels **d**–**f** are from the nodular zone. In the anterior cerebellum, **A** the amplitude of injected current required to elicit depolarization block was significantly reduced in SCA3 ASO-5 compared with that in WT Veh. **b** In response to depolarizing current, SCA3 Veh Purkinje neurons fire a greater number of action potentials than WT Veh neurons, while SCA3 ASO-5 neurons showed a decreased firing response to depolarizing current. **c** Input resistance was not altered among all groups. In the nodular zone, **d** the amplitude of injected current required to elicit depolarization block was significantly reduced in SCA3 Veh neurons compared with WT Veh, while SCA3 ASO-5 neurons were not significantly different from either group. **e** SCA3 Veh Purkinje neurons showed an increased firing response to depolarizing current compared with WT Veh, while SCA3 ASO-5 neurons were restored to near WT levels. **f** Input resistance was increased in both SCA3 groups compared with WT Veh, but ASO-5 treatment did not affect input resistance in SCA3 neurons. * = $p < 0.05$, ** = $p < 0.01$, *** = $p < 0.001$, one-way ANOVA with Holm-Sidak test for multiple comparisons, except in **b** and **e**, using two-way repeated-measures ANOVA with Tukey correction for multiple comparisons

block was mitigated in SCA3 ASO-5 neurons (Fig. 3d). SCA3 Veh Purkinje neurons were also more responsive to depolarizing current injection than WT Veh neurons, and this effect was restored to WT levels in SCA3 ASO-5 mice (Fig. 3e). Input resistance was significantly increased in both SCA3 groups compared with that in WT Veh, although input resistance was not changed between SCA3 Veh and SCA3 ASO-5 (Fig. 3f). Taken together, these data suggest an increase in Purkinje neuron excitability in SCA3 mice with no large changes in action potential waveform, while ASO-5 treatment restores excitability to WT levels. At 16 weeks, these changes are similar in both the anterior cerebellum and nodular zone.

Antisense Oligonucleotides Improve Motor Dysfunction in SCA3 Mice

Previous studies have demonstrated effective knockdown of disease-causing ATXN3 in SCA3 mice following delivery of an anti-*ATXN3* ASO. ATXN3 mRNA and protein knockdown is well tolerated and results in a significant, sustained improvement in motor dysfunction [8]. We aimed to determine whether improved Purkinje neuron hyperexcitability by ASO-5 correlates with improvement in the observed motor phenotype at 16 weeks of age, when K_V-related Purkinje neuron hyperexcitability is observed in SCA3 mice (Fig. 3). Using open-field assessment, we measured total locomotor activity (*x*–*y*-beam breaks) and total rearing activity (*z*-beam breaks) at 16 weeks of age. SCA3 Veh mice were significantly less active than WT Veh mice, and locomotion was restored to WT levels in SCA3 ASO-5 mice (Fig. 4a). Rearing activity did not differ significantly across all groups (Fig. 4b). These results indicate that ASO-5 treatment effectively rescues impairments in locomotor activity at a time when K_V channel dysfunction is observed in SCA3 mice.

Alterations in Purkinje Neuron Physiology Persist in Aged SCA3 Mice

While reduced $K_V1.6$ and $K_V3.3$ channel mRNA transcripts appear to contribute most directly to Purkinje neuron hyperexcitability in SCA3 mice at 16 weeks of age (Fig. 3), RNA sequencing data suggest that broader changes in K_V channel mRNA transcripts are present at 65 weeks of age (Fig. 1). We sought to determine whether these more widespread

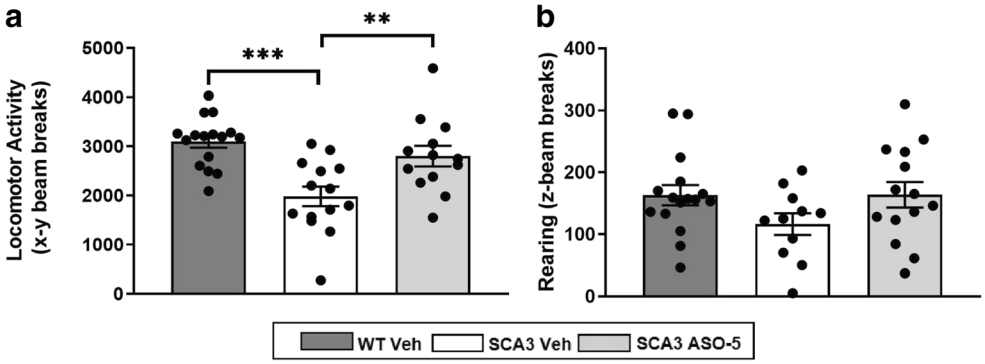

Fig. 4 Antisense oligonucleotide treatment rescues locomotor activity in SCA3 mice. **a** Total locomotor activity was significantly decreased in vehicle-treated SCA3 mice compared with vehicle-treated WT, while locomotion is restored to WT levels in ASO-5-treated SCA3 mice. **b** Rearing activity was not significantly altered among all groups. ** = $p < 0.01$, *** = $p < 0.001$, one-way ANOVA with Holm-Sidak correction for multiple comparisons

reductions in K_V channel transcripts result in more prominent Purkinje neuron dysfunction in late-stage SCA3 mice.

We performed patch-clamp recordings from acute cerebellar slices in WT and SCA3 mice at 65 weeks of age. While firing frequency was unchanged in the anterior cerebellum, it was surprisingly increased in the nodular zone of SCA3 mice (Fig. 5a). This is unexpected, as K_V channel dysfunction is more likely to result in reduced firing frequencies [34]. Similarly, the CV of the ISI was not significantly altered in either region of the cerebellum (Fig. 5b). We observed a similar enhanced response to depolarizing current injection in 65-week-old SCA3 mice as in 16-week-old mice, in both the anterior cerebellar lobules (Fig. 5c) and nodular zone (Fig. 5d), although this did not quite reach threshold of statistical significance in the nodular zone ($p = 0.054$). Additionally, the threshold of injected current to elicit depolarization block was reduced in SCA3 mice in both cerebellar regions (Fig. 5e). There was no significant difference in Purkinje neuron input resistance in either anterior cerebellum or nodular zone at this age, although a small sample size may underestimate a potential difference (Fig. 5f). These results show that alterations in Purkinje neuron excitability persist in aged SCA3 mice, but the amplitude of changes does not differ substantially from those observed in early symptomatic mice (16 weeks of age). Thus, the progressively worsened motor function seen over time in SCA3 mice appears not to be explained by progressive functional impairments of the cerebellar cortex, despite the wider spread changes in expression of K_V channels in aged SCA3 mice.

Discussion

Progressive neurodegeneration is observed across multiple brain regions in SCA3, most prominently in regions beyond the cerebellar cortex. However, it remains unclear whether cerebellar cortical dysfunction is an essential target for disease-modifying SCA3 therapy. In this study, we aimed to assess cerebellar Purkinje neuron involvement in SCA3 and explore whether it is a target for gene suppression strategies. In mouse models of SCAs 1, 2, 3, 6, and 7, cerebellar Purkinje neuron dysfunction coincides with early changes in motor function [11–16]. Previous studies in SCA3 mice suggest a role for potassium channel dysfunction in abnormal Purkinje neuron firing [8, 14]. The current study shows similar potassium channel dysfunction associated with cerebellar Purkinje neuron firing abnormalities in a mouse model of SCA3. ASO treatment improves motor activity and restores Purkinje neuron excitability in SCA3 mice at an early stage of the disease. However, Purkinje neuron dysfunction does not appear to be progressive in aged SCA3 mice despite progressively worsened motor impairment [29]. Together, these data suggest that altered Purkinje neuron intrinsic excitability likely contributes to motor impairment in SCA3 mice but is not the sole driver of progressive motor dysfunction that is rescued by ASO therapy.

Although no effective therapies for SCA3 are currently available, previous work demonstrates that sustained ASO-mediated knockdown of mutant and endogenous ATXN3 improves motor performance and is well tolerated in SCA3 mice [8]. However, biomarker readouts of neuronal dysfunction will be needed to track target engagement in SCA3 patients. One such biomarker, MRI, may be useful for tracking volume loss of vulnerable regions in SCA3, and preservation of brain volume may be a surrogate for slowing of neurodegeneration and target engagement [36–38]. Despite prominent cerebellar symptoms and signs in SCA3, it will be challenging to use cerebellar cortical volume as a readout of effectiveness of disease-modifying therapy due to the relative preservation of Purkinje neurons in SCA3 [1, 4, 5]. Recently, magnetic resonance spectroscopy (MRS) was used to identify changes in metabolite profiles in the cerebellar cortex in several mouse models of SCA1 prior to Purkinje neuron degeneration [39, 40]. Importantly, these MRS changes were identified at time

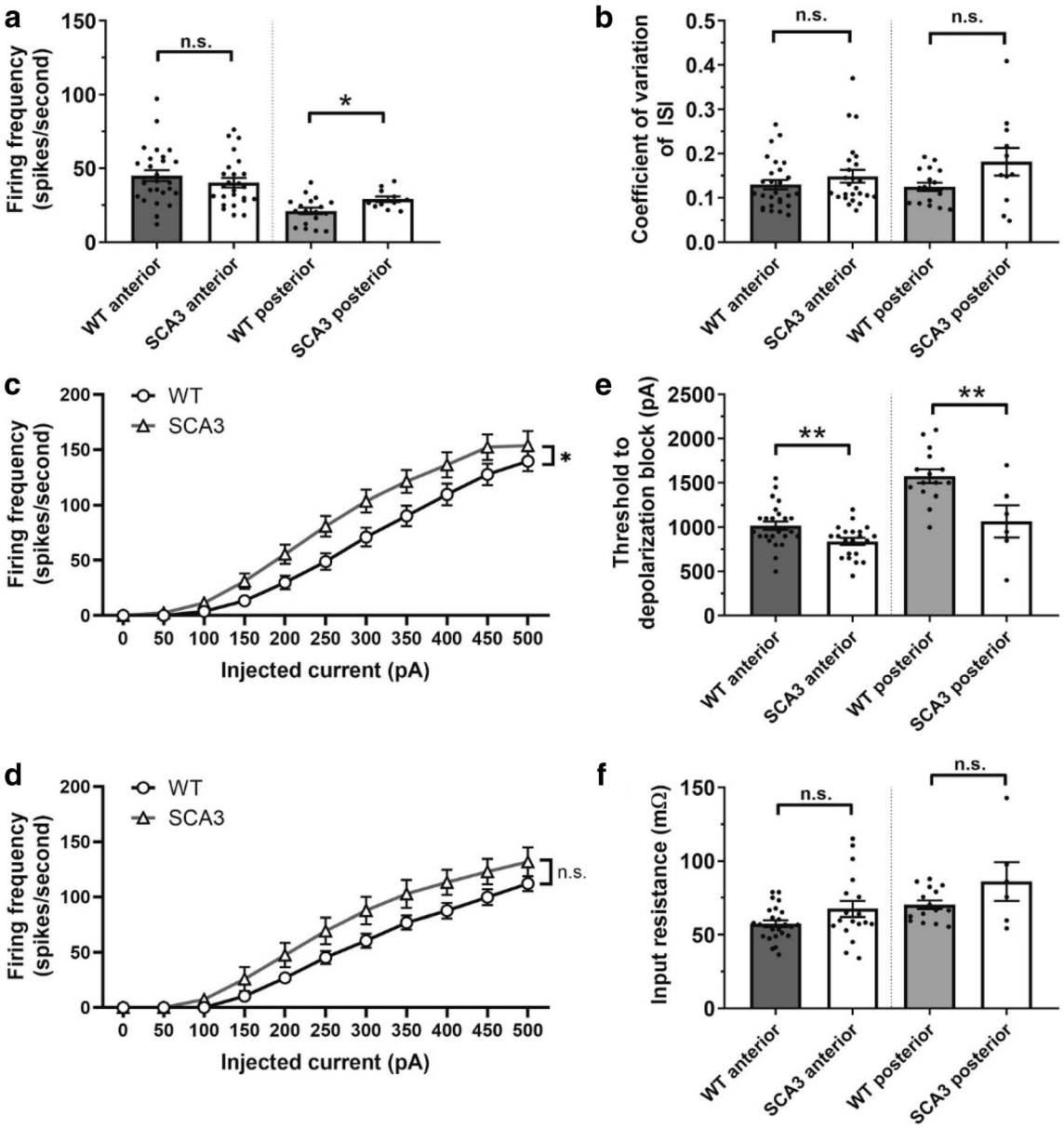

Fig. 5 Purkinje neuron dysfunction persists in late symptomatic SCA3 mice. Patch-clamp recordings were performed in vehicle-treated WT, vehicle-treated SCA3, and ASO-5-treated SCA3 mice at 15 months of age. **a** Purkinje neuron firing frequency is increased in the posterior cerebellar lobules, but not anterior cerebellar lobules, of SCA3 mice. **b** The regularity of spiking is not significantly changed between SCA3 and WT neurons in either anterior or posterior cerebellum. **c** The increased spiking response to depolarizing current persists in SCA3 Purkinje neurons at 15 months of age in the anterior cerebellum, although this did not reach statistical significance in the posterior cerebellum (**d**). **e** The threshold of injected current to elicit depolarization block was significantly reduced in SCA3 Purkinje neurons compared with that in WT in both regions of the cerebellum. **f** Input resistance was not significantly altered in either anterior or posterior cerebellum at this age. * = $p < 0.05$, ** = $p < 0.01$, two-tailed Student's t test or two-way repeated-measures ANOVA with Holm-Sidak correction for multiple comparisons in **c** and **d**

points at which we have noted prominent changes in physiology in the same SCA1 models [11, 20]. The neurochemical abnormalities detected by MRS were reversed in the cerebellum of ASO-treated SCA1 mice [41]. These MRS changes in SCA1 are relevant to human disease as the changes seen in murine models of SCA1 are similar to those seen in human SCA1 patients [42]. MRS alterations in the cerebellum are also noted in humans with SCA3, including in mutation carriers without prominent motor symptoms [43, 44]. These altered metabolite profiles are similar to changes detected in the same mouse model of SCA3 used in the current study [45]. Although the exact relationship between changes in neuronal metabolites measured using MRS and changes in Purkinje neuron physiology is not known, it is possible that cerebellar MRS profiles in SCA3 reflect the altered spiking measured by patch-clamp electrophysiology of cerebellar Purkinje neurons.

Given the reversibility of the changes in Purkinje neuron spiking with ASO therapy in the current study, if MRS does in fact correlate with changes in physiology, it may be possible to use improvement in MRS changes as an endpoint in clinical trials for target engagement, allowing for smaller sample sizes.

Despite a reduction in K_V channel expression in SCA3 Purkinje neurons, it remains unclear whether the observed Purkinje neuron hyperexcitability in SCA3 mice can be explained solely by $K_V1.6$ and $K_V3.3$ channel dysfunction. While the findings in the current study replicate physiological alterations noted in a previous study of SCA3 mice, including a reduced threshold to elicit depolarization block of spiking and an increased slope of the input-output curve to depolarization [14], the relationship between K_V channel dysfunction and the observed Purkinje neuron hyperexcitability may require further exploration. $K_V3.3$ knockout mice exhibit spike broadening due to reduced current during the repolarization phase of the action potential [33], which slows simple spike firing frequency and flattens the input-output curve in response to depolarizing current [34]. This contrasts with observations in SCA3 mice in the present study, where spike shape was unaffected and the slope of the input-output curve in response to depolarizing current was increased (Fig. 3). It is possible, however, that partial loss of both $K_V1.6$ and $K_V3.3$ reduces the shunt potassium current during the interspike interval, without affecting spike repolarization, to mediate the increase in excitability. Alternatively, indirect involvement of calcium-activated potassium channels, whose transcripts are not altered, or alterations in other depolarizing conductances, may contribute to the hyperexcitability phenotype. Future studies modeling the effect of partial loss of several K_V channels may reveal the exact mechanism for hyperexcitability in Purkinje neurons in SCA3 mice.

An interesting observation in late symptomatic SCA3 mice is the progressive worsening of motor symptoms despite minimal additional changes in Purkinje neuron excitability. RNA sequencing data in late-stage SCA3 mice shows reduced expression of K_V channel transcripts for five of six genes (Fig. 1), indicating reduced transcript expression in whole cerebellar tissue. Analysis of in situ hybridization data from wild-type mice shows enriched expression of these ion channel genes in the Purkinje neuron layer when compared with that in the granule cell layer, particularly for the anterior cerebellar lobules. However, these data also indicate that molecular layer interneurons in the cerebellar cortex and structures outside of the cerebellar cortex, namely the medial cerebellar nuclei and pontine gray matter, also express many of these ion channel genes at detectable levels. Additionally, $K_v1.1$, which causes episodic ataxia type 1 [46], and $K_v1.2$ are known to be highly expressed on basket cell pinceau, a major inhibitory cell type that directly influences Purkinje neuron function [47, 48]. It is possible that progressive worsening of motor function in SCA3 mice reflects additional neuronal dysfunction of these structures in the late-stage disease. While many of these areas project to the cerebellum directly or indirectly [31], and would be expected to worsen Purkinje neuron dysfunction through altered synaptic input to Purkinje neurons, assessment of Purkinje neuron intrinsic excitability in cerebellar slices as performed in the current study would underestimate the Purkinje neuron dysfunction not directly due to changes in ion channel expression and function in Purkinje neurons. Network-level changes in function due to altered excitability in neurons that ultimately converge on Purkinje neurons may therefore explain the worsened cerebellar dysfunction late in disease.

In SCA3 patients, disease progression is variable with CAG repeat length, accounting for some of the variability in age of onset [49]. Similarly, in mouse models of SCA3 and other polyglutamine SCAs, gene dosing appears to significantly impact disease phenotypes particularly related to age-of-onset and progression of motor impairment [15, 18, 50]. Interestingly, the present study suggests that genotype may impact specific physiological alterations in SCA3. Purkinje neuron firing abnormalities differ between the homozygous SCA3 mice of this study and hemizygous SCA3 mice in a previous report, which found that Purkinje neuron firing frequency was reduced in association with increased depth of the AHP [8]. The hemizygous SCA3 phenotype is more closely reminiscent of what occurs with isolated $K_V3.3$ dysfunction [34], whereas the additional involvement of $K_V1.6$ in homozygous SCA3 mice may produce distinct alterations in membrane excitability. This suggests an interesting possibility: increasing mutant gene dosage may not only produce quantitative changes in individual transcripts but also recruit additional novel changes in transcription. Increasing CAG repeat length may similarly result in different physiology in both mouse models and human SCA3, due to altered transcriptional profiles of ion channels. Genetic variability could potentially complicate therapies that rely on targeting specific ion channels for treatment of symptoms in SCA3.

Conclusion

There is an increasing need to define specific readouts of neuronal involvement in degenerative disorders as gene suppression–based therapies move into clinical use. In this study, we have presented evidence that cerebellar Purkinje neuron dysfunction is present and relevant in a mouse model of SCA3 early in disease. ASO-mediated reduction of ATXN3 was able to rectify the underlying changes in the expression of K_V channels and improve Purkinje neuron physiology, suggesting that these molecular and electrophysiological features could serve as potential readouts of target engagement by ASO therapy. The non-progressive nature of changes in Purkinje neuron physiology, in contrast to the

progressive motor phenotype in SCA3 mice, implies that anti-ATXN3 ASO therapy targets additional neuronal circuits beyond the cerebellar cortex to mitigate these progressive motor behavioral changes.

Acknowledgments We thank Ionis Pharmaceuticals for providing ASO-5 for these studies. We thank Haoran Huang and Kate Blumenstein for the technical support.

Funding Information This work was funded by NINDS U01 NS106670 (HSM, HLP) and R01NS085054 (VGS).

Compliance with Ethical Standards

All animal procedures were approved by the University of Michigan Institutional Animal Care and Use Committee (IACUC). Procedures were conducted in accordance with the U.S. Public Health Service's Policy on Humane Care and Use of Laboratory Animals.

Conflict of Interest The authors declare that they have no conflict of interest.

References

1. Durr A. Autosomal dominant cerebellar ataxias: polyglutamine expansions and beyond. Lancet Neurol. 2010;9(9):885–94.
2. Gardiner SL, Boogaard MW, Trompet S, de Mutsert R, Rosendaal FR, Gussekloo J, et al. Prevalence of carriers of intermediate and pathological polyglutamine disease-associated alleles among large population-based cohorts. JAMA Neurol. 2019;76(6):650–6.
3. McLoughlin HS, Moore LR, Paulson HL. Pathogenesis of SCA3 and implications for other polyglutamine diseases. Neurobiol Dis. 2020;134:104635.
4. Seidel K, Siswanto S, Brunt ERP, den Dunnen W, Korf HW, Rub U. Brain pathology of spinocerebellar ataxias. Acta Neuropathol. 2012;124(1):1–21.
5. Rub U, Schols L, Paulson H, Auburger G, Kermer P, Jen JC, et al. Clinical features, neurogenetics and neuropathology of the polyglutamine spinocerebellar ataxias type 1, 2, 3, 6 and 7. Prog Neurobiol. 2013;104:38–66.
6. Paulson HL, Shakkottai VG, Clark HB, Orr HT. Polyglutamine spinocerebellar ataxias - from genes to potential treatments. Nat Rev Neurosci. 2017;18(10):613–26.
7. Switonski PM, Fiszer A, Kazmierska K, Kurpisz M, Krzyzosiak WJ, Figiel M. Mouse ataxin-3 functional knock-out model. NeuroMolecular Med. 2011;13(1):54–65.
8. McLoughlin HS, Moore LR, Chopra R, Komlo R, McKenzie M, Blumenstein KG, et al. Oligonucleotide therapy mitigates disease in spinocerebellar ataxia type 3 mice. Ann Neurol. 2018;84(1):64–77.
9. Moore LR, Rajpal G, Dillingham IT, Qutob M, Blumenstein KG, Gattis D, et al. Evaluation of antisense oligonucleotides targeting ATXN3 in SCA3 mouse models. Mol Ther-Nucl Acids. 2017;7:200–10.
10. Toonen LJA, Rigo F, van Attikum H, van Roon-Mom WMC. Antisense oligonucleotide-mediated removal of the polyglutamine repeat in spinocerebellar ataxia type 3 mice. Mol Ther-Nucl Acids. 2017;8:232–42.
11. Dell'Orco JM, Wasserman AH, Chopra R, Ingram MAC, Hu YS, Singh V, et al. Neuronal atrophy early in degenerative ataxia is a compensatory mechanism to regulate membrane excitability. J Neurosci. 2015;35(32):11292–307.
12. Dell'Orco JM, Pulst SM, Shakkottai VG. Potassium channel dysfunction underlies Purkinje neuron spiking abnormalities in spinocerebellar ataxia type 2. Hum Mol Genet. 2017;26(20):3935–45.
13. Hansen ST, Meera P, Otis TS, Pulst SM. Changes in Purkinje cell firing and gene expression precede behavioral pathology in a mouse model of SCA2. Hum Mol Genet. 2013;22(2):271–83.
14. Shakkottai VG, do Carmo Costa M, Dell'Orco JM, Sankaranarayanan A, Wulff H, Paulson HL. Early changes in cerebellar physiology accompany motor dysfunction in the polyglutamine disease spinocerebellar ataxia type 3. J Neurosci. 2011;31(36):13002–14.
15. Jayabal S, Chang HH, Cullen KE, Watt AJ. 4-aminopyridine reverses ataxia and cerebellar firing deficiency in a mouse model of spinocerebellar ataxia type 6. Sci Rep. 2016;6:29489.
16. Stoyas CA, Bushart DD, Switonski PM, Ward JM, Alaghatta A, Tang MB, et al. Nicotinamide pathway-dependent Sirt1 activation restores calcium homeostasis to achieve neuroprotection in spinocerebellar ataxia type 7. Neuron. 2020;105(4):630–+.
17. Bushart DD, Shakkottai VG. Ion channel dysfunction in cerebellar ataxia. Neurosci Lett. 2019;688:41–8.
18. Cemal CK, Carroll CJ, Lawrence L, Lowrie MB, Ruddle P, Al-Mahdawi S, et al. YAC transgenic mice carrying pathological alleles of the MJD1 locus exhibit a mild and slowly progressive cerebellar deficit. Hum Mol Genet. 2002;11(9):1075–94.
19. © 2004 Allen Institute for Brain Science, Allen Mouse Brain Atlas. Available from: mouse.brain-map.org, Lein ES, Hawrylycz MJ, Ao N, Ayres M, et al. Genome-wide atlas of gene expression in the adult mouse brain. Nature. 2007;445(7124):168–76.
20. Bushart DD, Chopra R, Singh V, Murphy GG, Wulff H, Shakkottai VG. Targeting potassium channels to treat cerebellar ataxia. Ann Clin Transl Neurol. 2018;5(3):297–314.
21. Chung YH, Shin C, Kim MJ, Lee BK, Cha CI. Immunohistochemical study on the distribution of six members of the Kv1 channel subunits in the rat cerebellum. Brain Res. 2001;895(1–2):173–7.
22. Serodio P, Rudy B. Differential expression of Kv4 K+ channel subunits mediating subthreshold transient K+ (A-type) currents in rat brain. J Neurophysiol. 1998;79(2):1081–91.
23. Southan AP, Robertson B. Electrophysiological characterization of voltage-gated K(+) currents in cerebellar basket and purkinje cells: Kv1 and Kv3 channel subfamilies are present in basket cell nerve terminals. J Neurosci. 2000;20(1):114–22.
24. Hurlock EC, Bose M, Pierce G, Joho RH. Rescue of motor coordination by Purkinje cell-targeted restoration of Kv3.3 channels in Kcnc3-null mice requires Kcnc1. J Neurosci. 2009;29(50):15735–44.
25. Browne DL, Gancher ST, Nutt JG, Brunt ER, Smith EA, Kramer P, et al. Episodic ataxia/myokymia syndrome is associated with point mutations in the human potassium channel gene, KCNA1. Nat Genet. 1994;8(2):136–40.
26. Waters MF, Minassian NA, Stevanin G, Figueroa KP, Bannister JP, Nolte D, et al. Mutations in voltage-gated potassium channel KCNC3 cause degenerative and developmental central nervous system phenotypes. Nat Genet. 2006;38(4):447–51.
27. Lee YC, Durr A, Majczenko K, Huang YH, Liu YC, Lien CC, et al. Mutations in KCND3 cause spinocerebellar ataxia type 22. Ann Neurol. 2012;72(6):859–69.
28. Duarri A, Jezierska J, Fokkens M, Meijer M, Schelhaas HJ, den Dunnen WF, et al. Mutations in potassium channel kcnd3 cause spinocerebellar ataxia type 19. Ann Neurol. 2012;72(6):870–80.
29. Costa Mdo C, Luna-Cancalon K, Fischer S, Ashraf NS, Ouyang M, Dharia RM, et al. Toward RNAi therapy for the polyglutamine disease Machado-Joseph disease. Mol Ther. 2013;21(10):1898–908.

30. Klockgether T, Mariotti C, Paulson HL. Spinocerebellar ataxia. Nat Rev Dis Primers. 2019;5(1):24.
31. It*o M. The cerebellum and neural control, vol. xvii. New York: Raven Press; 1984. p. 580.
32. Zhou H, Lin Z, Voges K, Ju C, Gao Z, Bosman LW, et al. Cerebellar modules operate at different frequencies. Elife. 2014;3: e02536.
33. McMahon A, Fowler SC, Perney TM, Akemann W, Knopfel T, Joho RH. Allele-dependent changes of olivocerebellar circuit properties in the absence of the voltage-gated potassium channels Kv3.1 and Kv3.3. Eur J Neurosci. 2004;19(12):3317–27.
34. Akemann W, Knopfel T. Interaction of Kv3 potassium channels and resurgent sodium current influences the rate of spontaneous firing of Purkinje neurons. J Neurosci. 2006;26(17):4602–12.
35. Zagha E, Manita S, Ross WN, Rudy B. Dendritic Kv3.3 potassium channels in cerebellar purkinje cells regulate generation and spatial dynamics of dendritic Ca2+ spikes. J Neurophysiol. 2010;103(6): 3516–25.
36. Stefanescu MR, Dohnalek M, Maderwald S, Thurling M, Minnerop M, Beck A, et al. Structural and functional MRI abnormalities of cerebellar cortex and nuclei in SCA3, SCA6 and Friedreich's ataxia. Brain. 2015;138(Pt 5):1182–97.
37. Rezende TJR, de Paiva JLR, Martinez ARM, Lopes-Cendes I, Pedroso JL, Barsottini OGP, et al. Structural signature of SCA3: from presymptomatic to late disease stages. Ann Neurol. 2018;84(3):401–8.
38. Ashizawa T, Oz G, Paulson HL. Spinocerebellar ataxias: prospects and challenges for therapy development. Nat Rev Neurol. 2018;14(10):590–605.
39. Emir UE, Brent Clark H, Vollmers ML, Eberly LE, Oz G. Noninvasive detection of neurochemical changes prior to overt pathology in a mouse model of spinocerebellar ataxia type 1. J Neurochem. 2013;127(5):660–8.
40. Oz G, Nelson CD, Koski DM, Henry PG, Marjanska M, Deelchand DK, et al. Noninvasive detection of presymptomatic and progressive neurodegeneration in a mouse model of spinocerebellar ataxia type 1. J Neurosci. 2010;30(10):3831–8.
41. Friedrich J, Kordasiewicz HB, O'Callaghan B, Handler HP, Wagener C, Duvick L, et al. Antisense oligonucleotide-mediated ataxin-1 reduction prolongs survival in SCA1 mice and reveals disease-associated transcriptome profiles. JCI Insight. 2018;3(21).
42. Deelchand DK, Joers JM, Ravishankar A, Lyu T, Emir UE, Hutter D, et al. Sensitivity of volumetric magnetic resonance imaging and magnetic resonance spectroscopy to progression of spinocerebellar ataxia type 1. Mov Disord Clin Pract. 2019;6(7):549–58.
43. Adanyeguh IM, Henry PG, Nguyen TM, Rinaldi D, Jauffret C, Valabregue R, et al. In vivo neurometabolic profiling in patients with spinocerebellar ataxia types 1, 2, 3, and 7. Mov Disord. 2015;30(5):662–70.
44. Joers JM, Deelchand DK, Lyu T, Emir UE, Hutter D, Gomez CM, et al. Neurochemical abnormalities in premanifest and early spinocerebellar ataxias. Ann Neurol. 2018;83(4):816–29.
45. Costa MC, Radzwion M, McLoughlin HS, Ashraf NS, Fischer S, Shakkottai VG, et al. In vivo molecular signatures of cerebellar pathology in spinocerebellar ataxia type 3. In: Mov Disord; 2020. https://doi.org/10.1002/mds.28140.
46. Adelman JP, Bond CT, Pessia M, Maylie J. Episodic ataxia results from voltage-dependent potassium channels with altered functions. Neuron. 1995;15(6):1449–54.
47. Laube G, Roper J, Pitt JC, Sewing S, Kistner U, Garner CC, et al. Ultrastructural localization of shaker-related potassium channel subunits and synapse-associated protein 90 to septate-like junctions in rat cerebellar Pinceaux. Brain Res Mol Brain Res. 1996;42(1): 51–61.
48. Kole MJ, Qian J, Waase MP, Klassen TL, Chen TT, Augustine GJ, et al. Selective loss of presynaptic potassium channel clusters at the cerebellar basket cell terminal pinceau in Adam11 mutants reveals their role in ephaptic control of Purkinje cell firing. J Neurosci. 2015;35(32):11433–44.
49. Tezenas du Montcel S, Durr A, Bauer P, Figueroa KP, Ichikawa Y, Brussino A, et al. Modulation of the age at onset in spinocerebellar ataxia by CAG tracts in various genes. Brain. 2014;137(Pt 9):2444–55.
50. Ramani B, Harris GM, Huang R, Seki T, Murphy GG, Carmo Costa MD, et al. A knockin mouse model of spinocerebellar ataxia type 3 exhibits prominent aggregate pathology and aberrant splicing of the disease gene transcript. Hum Mol Genet. 2017;26(16): 3232–3.